21th International Conference on Renewable Energies and Power Quality (ICREPQ'23)
Madrid (Spain), 24th to 26th May 2023
Renewable Energy and Power Quality Journal (RE&PQJ)
ISSN 2172-038 X, Volume No.21, July 2023

Analytical Design Methodology for Wind Power Permanent Magnet Synchronous Generators

V. Ballestín-Bernad, J. S. Artal-Sevil, J. A. Domínguez-Navarro

Department of Electrical Engineering
School of Engineering and Architecture, University of Zaragoza
Campus Río Ebro – C/ María de Luna, 3, 50018 Zaragoza (Spain)
Phone number: +0034 976 842823, e-mail: ballestin@unizar.es, jsartal@unizar.es, jadona@unizar.es

Abstract. In this paper a novel analytical design methodology for wind power permanent magnet synchronous generators is presented. This kind of electric generator plays a major role in small-scale wind energy conversion systems up to 10 kW. The proposed diameter-cubed sizing equation is based both on the generator requirements, imposed by the application, and the design parameters that rely on the designer criteria. The magnetic field waveforms of both the permanent magnets field and the armature field are considered from the first moment through the winding factors, as well as the slots effects given by the Carter factor. The analytical model of the permanent magnet synchronous generator is validated with the finite element method, showing good agreement, both with no load and under load. As the generator is unsaturated, the main source of divergence between the analytical and the finite element model are the iron losses, due to the non-uniform magnetic field distribution.

Keywords. Wind power, Permanent magnet synchronous generators, Analytical design, Finite element method

1. Introduction

Small-scale wind energy conversion systems (WECS) have a great potential to supply power in rural areas, as the availability of wind resources and land is usually higher in remote locations than in the vicinity of big cities. As WECS use only a small fraction of the land, their settlement is compatible with other uses such as agriculture or extensive farming.

Fig. 1 illustrates a comparison between different wind turbines, according to their rated power and the rotor diameter. Large-scale wind farms and large-scale wind turbines seem to have an impact on climatic conditions, both on temperature [2] and precipitations [3], therefore small-scale, decentralized WECS emerge as a more sustainable solution for renewable energy production. However, the optimization of the initial cost per watt and the unit cost per kilowatt-hour is a great challenge for small-scale WECS [4]. Both horizontal- and vertical-axis wind turbines can be used for this purpose.

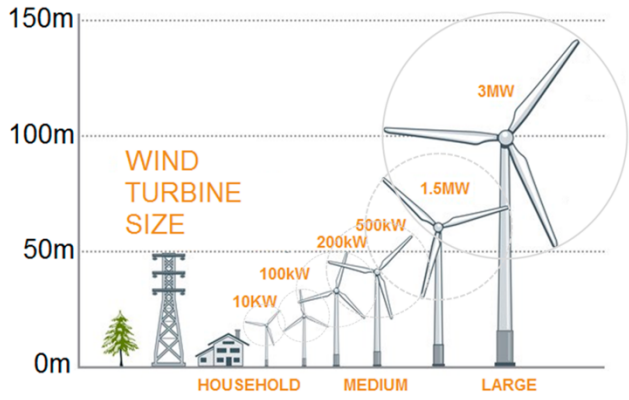

Fig. 1. Representative size and power of wind turbines [1]

WECS are mostly based on induction generators (IGs) and synchronous generators (SGs). IGs always require a multi-stage gearbox to transform the rotation speed of the wind turbine into higher values. IGs are usually divided into squirrel-cage generators and doubly-fed generators: the former has a limited, non-controllable speed range and consume reactive power, whereas the latter requires brushes and expensive power converters that are very sensitive to over currents [5]. Besides, SGs can operate at variable speed, and even as direct-drive systems. They are divided into electrically-excited synchronous generators or permanent magnet synchronous generators (PMSGs). Permanent magnet generators are preferred for small-scale WECS up to 10 kW, as there is no need for commutators, slip rings or brushes [6], but the use of an AC-DC power converter becomes mandatory as the output voltage of the generator is variable both in amplitude and frequency. Then the resultant DC power can be either directly used (in a DC load or battery) or inverted with a DC-AC converter to feed AC loads or the utility grid. In [7] a discussion about the power converter schemes for small-scale WECS is presented, and the power converter topologies are classified according to the isolation transformer and the generator side rectifier.

Among the PMSGs, different topologies haven been proposed in literature in the field of small-scale renewable energy generation. In addition to conventional radial flux machines (RFMs) with surface or inner magnets, axial flux machines (AFMs) and transverse flux machines (TFMs) are gaining wider attention due to their high power and/or torque density, at the cost of more cumbersome assembly and manufacturing. In [8] a single-phase, single-side, 1 kW axial flux permanent magnet generator (AFPMG) is proposed for the utilization of hydro energy in remote locations. A larger 20 kW, three-phase, double-sided version of the AFPMG is presented in [9]. Due to reports of corrosion in small-scale WECS with neodymium magnets, ferrite magnets are used in an 850 W AFPMG in [10]. Two case studies for local manufacturing of small-scale WECS based on AFPMGs are presented in [11]. Coreless AFPMGs based on additive manufacturing have been also investigated for local manufacturing, both in its double-rotor [12] and single-rotor [13] versions. In [14] the RFM and AFM are compared for micro-wind-turbine applications and the analysis shows that the RFM exhibits lower active materials cost than the AFM. Besides, TFMs potentially enables higher torque than the RFMs in the low-kW range, but their scalability must be further investigated [15].

Recycling of electrical machines is progressively becoming more important when designing an electrical generator for small-scale WECS. In [16] the feasibility of using an automotive claw-pole alternator for small wind turbines is demonstrated, comparing both the energy yield and the energy cost with some commercial systems. In [17] the rotor of a claw-pole alternator is used together with a conventional stator to build a small PMSG for wind energy harvesting. It is shown that different PM arrangements on the rotor lead to different torques and efficiencies [18].

In this paper a design methodology for a PMSGs intended for small-scale WECS is proposed. The radial flux topology has been chosen because, according to literature, it shows the lowest cost of active materials, better mechanical stability and easier recycling due to higher availability. Furthermore, the sizing equations proposed here could be adapted to axial and transverse flux topologies changing only a few design parameters. In Section 2 the specifications and design parameters of the PMSG are shown. In Section 3 the analytical sizing equations are presented, and a parametric study is conducted both on the stator outer diameter and power density. Finally, in Section 4 the analytical model is validated with the finite element method (FEM) using FluxMotor from Altair.

2. PMSG Main Specifications and Design Parameters

Table I shows the main specifications, or rated values, of the PMSG, imposed by the small-scale wind power application requirements. Besides, Table II shows the design parameters that are needed for the machine sizing according to the designer criteria, grouped by their location and their effect on the machine geometry (overall geometry, rotor and stator). Only the fundamental harmonics will be considered in this work.

Table I. - Main specifications of the PMSG

SPECIFICATION	SYMBOL	VALUE
Power (kW)	P	10
Frequency (Hz)	f	50
Number of phases	m	3
Wind turbine speed (rpm)	n_{wt}	20
Gearbox steps		3
Line voltage (V)	U_{line}	400
Power factor	$\cos\varphi$	0.80

Table II. - Design parameters of the PMSG

GROUP	PARAMETER	SYMBOL	VALUE
Overall geometry and loads	Number of pole pairs	p	5
	Axial length to gap diameter ratio	k_l	1.50
	Current load (A/m)	A	20000
	Back-EMF to voltage ratio	ε	1.3
Rotor PMs	PM span	θ_m	150°
	Remanence of PMs (T)	B_m	1.11
	Relative permeability of PMs	μ_{rm}	1.10
	PM to air gap height ratio	k_{gm}	4
Stator winding and slots	Pitch shortage angle		0
	Slots per pole and phase	q	2
	Slot opening to slot pitch ratio	k_{so1}	0.10
	Air gap to slot opening ratio	k_{so2}	0.60
	Current density (A/mm^2)	J	6
	Conductors per turn	Z_t	2
	Fill factor	k_{fill}	0.4

The generator power (P) follows (1), where E_{01} is the RMS value of the first harmonic of the phase-to-neutral back electromotive force (back-EMF) and I_q is the RMS sinusoidal q-axis current (therefore the I_q and E_{01} phasors are aligned).

$$P = mE_{01}I_q \tag{1}$$

On the one hand, the phase back-EMF is related to the phase voltage (U) through the back-EMF to voltage ratio (2,3). On the other hand, the back-EMF is a function of the RMS value of the first harmonic of the no-load flux linkage (ψ_{01}) (4). ω is the electrical speed of the machine in radians per second (5) and ψ_{01} depends on the PMs remanence, waveform and section, as shown in Section 3.

$$U = \frac{U_{line}}{\sqrt{3}} \tag{2}$$

$$\varepsilon = \frac{E_{01}}{U} \tag{3}$$

$$E_{01} = \omega\psi_{01} \tag{4}$$

$$\omega = 2\,\pi f \tag{5}$$

The q-axis current in (1) can be expressed as a function of the current load (6), where N_m is the number of turns per phase and D_g is the air gap diameter.

$$A = \frac{2mN_m I_q}{\pi D_g} \tag{6}$$

Finally, if the copper loses are neglected, the rated current (I) of the machine can be obtained by (7).

$$P = mUI\cos\varphi \tag{7}$$

3. Analytical Sizing Equations

The analytical design methodology proposed in this paper is formed by several sequential steps. First, the PMs magnetomotive force (MMF) and the armature MMF are characterized through the PMs/winding factors. After that, a diameter-cubed sizing equation is proposed for the air gap diameter calculation, then the no-load MMF and the no-load flux linkage can be fully characterized. Then the stator winding (slots and coils) is designed, checking the magnetic saturation, and the overall diameters are obtained. Finally, the efficiency of the machine is evaluated calculating copper and iron losses.

A. PMs and Armature Field

Permanent magnets are equivalent to DC field-windings, as both create a static, constant MMF. Therefore, the winding factor concept can be equally applied to PMs and coils.

The PMs span (θ_m) is usually lower than 180 electrical degrees in order to reduce the leakage flux between adjacent magnets, so the pitch factor of PMs (ξ_{fp}) follows (8). The PMs factor (ξ_f) equals the PMs pitch factor. Besides, in this work a full-pitch, distributed winding is proposed for the stator armature winding, so the pitch factor of the armature winding equals 1 and the distribution factor (ξ_{ad}) follows (9,10). Finally, the armature winding factor (ξ_a) is calculated as the product of the pitch factor and the distribution factor.

$$\xi_{fp} = \cos\frac{180°-\theta_m}{2} \tag{8}$$

$$\gamma_e = \frac{180°}{mq} \tag{9}$$

$$\xi_{ad} = \frac{\sin\frac{q\gamma_e}{2}}{q\sin\frac{\gamma_e}{2}} \tag{10}$$

When applying the Ampère's Law to a symmetrical magnetic path that crosses the air gap, the peak value of the no-load flux density ($\hat{B}_g$) produced by PMs can be obtained from the rotor PMs design parameters and the Carter factor (11,12,13). g_m is the PMs radial length and g_a is the air gap length.

$$k_{gm} = g_m/g_a \tag{11}$$

$$k_C = \frac{k_{so1}^{-1}}{k_{so1}^{-1} - \frac{k_{so2}^{-1}}{5+k_{so2}^{-1}}} \tag{12}$$

$$\hat{B}_g = B_m \frac{\frac{k_{gm}}{\mu_{rm}}}{\frac{k_{gm}}{\mu_{rm}}+k_C} \tag{13}$$

If the no-load flux density waveform is assumed to be rectangular, the peak value of its first harmonic ($\hat{B}_{g1}$) follows (14), and the mean value ($\bar{B}_{g1}$) follows (15).

$$\hat{B}_{g1} = \frac{4}{\pi}\hat{B}_g\xi_f \tag{14}$$

$$\bar{B}_{g1} = \frac{2}{\pi}\hat{B}_{g1} \tag{15}$$

Finally, the RMS value of the no-load flux linkage is given by (16,17), where S_p is the pole surface.

$$S_p = \frac{\pi D_g^2 k_l}{2p} \tag{16}$$

$$\psi_{01} = \frac{1}{\sqrt{2}}N_m\bar{B}_{g1}S_p\xi_a \tag{17}$$

B. Diameter-cubed Sizing Equation

Putting together (1), (4-6) and (14-17), the diameter-cubed sizing equation is obtained (18). Results are shown in Table III.

$$D_g = \sqrt[3]{\frac{\frac{1}{2\pi\sqrt{2}}\,P\,p}{f\,\xi_f\,\hat{B}_g\,\xi_a\,A\,k_l}} \tag{18}$$

Table III. - Results of the PMs field, the armature field and the diameter-cubed equation calculations

MAGNITUDE	SYMBOL	VALUE
PMs factor	ξ_f	0.966
Armature winding factor	ξ_a	0.966
Carter factor	k_C	1.026
No-load air gap B, peak (T)	$\hat{B}_g$	0.866
No-load air gap B, 1st harmonic, peak (T)	$\hat{B}_{g1}$	1.065
No-load air gap B, mean (T)	$\bar{B}_{g1}$	0.678
Air gap diameter (mm)	D_g	167.1
Axial length (mm)	L_{axial}	250.6
No-load flux linkage, RMS (Wb)	ψ_{01}	0.9556
Number of turns per phase	N_m	160

Besides, from the definition of the number of slots per pole and phase (19) and the slot pitch τ_Q (20), the slot opening width (w_{so}), the tooth shoe width (w_{ts}), the air gap length and the PMs length can be obtained (21,22,23,24).

$$q = \frac{Q}{2mp} \tag{19}$$

$$\tau_Q = \frac{\pi D_g}{Q} \quad (20)$$

$$w_{so} = k_{so1}\tau_Q \quad (21)$$

$$w_{ts} = \tau_Q - w_{so} \quad (22)$$

$$g_a = k_{so1}k_{so2}\tau_Q \quad (23)$$

$$g_m = k_{gm}g_a \quad (24)$$

Some of the most representative dimensions of the PMSM have been depicted in Fig. 2 and Fig. 3. In the proposed PMSM the slots have parallel sides, so the slot width is constant.

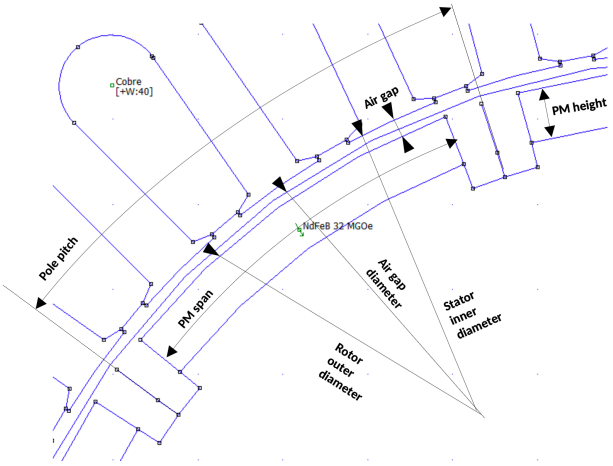

Fig. 2. Main dimensions of the rotor and the air gap

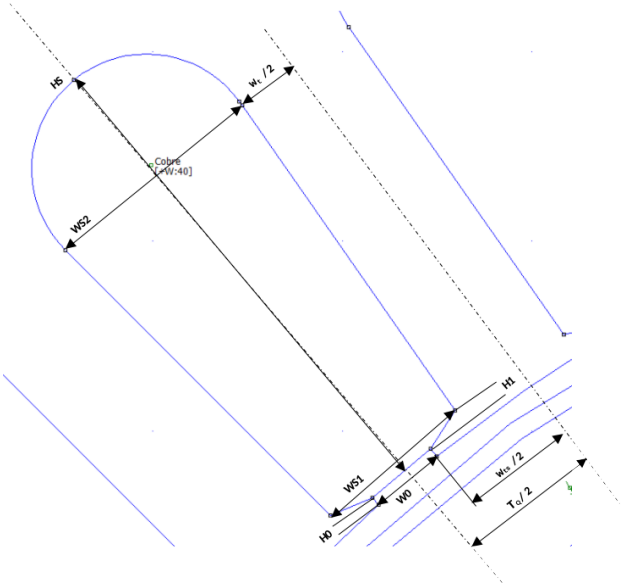

Fig. 3. Main dimensions of the stator

C. Stator Winding Design

The turn section (S_t) is given by the rated current and the current density (25). The wire diameter (D_w) follows (26), the number of turns per coil (N_c) follows (27) and the slot section (S_s) follows (28).

$$S_t = \frac{I}{J} \quad (25)$$

$$D_w = \sqrt{\frac{4\,S_t}{\pi\,Z_t}} \quad (26)$$

$$N_c = \frac{N_m}{pq} \quad (27)$$

$$S_s = \frac{N_c\,S_t}{k_{fill}} \quad (28)$$

Then the slot width (w_s) and the tooth width (w_t) are set as half of the slot pitch (29) and the slot opening height (h_{so}) is set as equal to the air gap length. Finally, the slot height (h_s) is calculated (30).

$$w_s = w_t = \frac{\tau_Q}{2} \quad (29)$$

$$h_s = \frac{S_s}{w_s} + h_{so} \quad (30)$$

D. Overall Diameters

Once the main dimensions of the rotor, air gap and stator are obtained, the rotor and stator yoke give the overall diameters. The rotor yoke (h_{ry}) and the stator yoke (h_{sy}) can be calculated regarding the magnetic saturation (31). In this work, the maximum flux density before saturation (B_{lim}) has been chosen as 1.0 T, according to the magnetic curves of the lamination material (M300-35A).

$$h_{ry} = h_{sy} = \frac{\psi_{01}/N_m}{2\,B_{lim}\,L_{axial}} \quad (31)$$

Then the stator outer diameter (D_{so}) and the rotor inner diameter (D_{ri}) can be calculated (32,33).

$$D_{so} = D_g + g_a + 2(h_s + h_{sy}) \quad (32)$$

$$D_{ri} = D_g - g_a - 2(g_m + h_{ry}) \quad (33)$$

Results are shown in Table IV.

Table IV. - Results of the stator winding design and overall diameters

MAGNITUDE	SYMBOL	VALUE
Slot pitch (mm)	τ_Q	8.8
Slot opening width (mm)	w_{so}	0.9
Tooth shoe width (mm)	w_{ts}	7.9
Air gap length (mm)	g_a	0.52
PMs radial length (mm)	g_m	2.1
Wire diameter (mm)	D_w	1.4
Slot width (mm)	w_s	4.4
Tooth width (mm)	w_t	4.4
Slot height (mm)	h_s	28.0
Rotor yoke height (mm)	h_{ry}	11.9
Stator yoke height (mm)	h_{sy}	11.9
Stator outer diameter (mm)	D_{so}	247.5
Rotor inner diameter (mm)	D_{ri}	138.5

E. *Losses and Efficiency*

Electrical machines losses are usually divided into copper losses and iron losses. Given the machine dimensions, the resistance per phase (R) is given by (34) and the copper losses (P_{Cu}) due to Joule effect follow (35). The length of one turn (L_t) must consider the end-winding length, that in this work has assumed as a semi-circumference. ρ_{Cu} is the copper resistivity.

$$R = \rho_{Cu} \frac{N_m L_t}{S_t} \tag{34}$$

$$P_{Cu} = mRI^2 \tag{35}$$

Besides, iron losses (P_{Fe}) are the sum of hysteresis losses $P_{Fe,h}$ (36) and eddy current losses $P_{Fe,e}$ (37). The main input data are: the iron volume (V_{Fe}), the frequency, the flux density and the lamination thickness (a). In this work the flux density has been assumed as equal to B_{lim} because the rotor and stator yoke fields will be close to this value. The material constants (k_h, α_h, k_e) have been taken from the FluxMotor materials library for M300-35A.

$$P_{Fe,h} = V_{Fe}\, k_h\, f\, {B_{lim}}^{\alpha_h} \tag{36}$$

$$P_{Fe,e} = V_{Fe}\, k_e\, (a\, f\, B_{lim})^2 \tag{37}$$

Finally, the generator efficiency follows (38). Results are shown in Table V.

$$\eta = 100 \frac{P - P_{Cu} - P_{Fe}}{P} \tag{38}$$

Table V. - Results of the losses and efficiency calculation

MAGNITUDE	SYMBOL	VALUE
Resistance per phase (ohm)	R	0.69
Copper losses (W)	P_{Cu}	673
Iron losses (W)	P_{Fe}	85
Efficiency (%)	η	92.4

F. *Parametric Study*

As the PMs remanence and current load are the most influent parameters on the machine sizing, their effects on the stator outer diameter and power density P_d (39) have been further investigated.

$$P_d = \frac{P}{\pi\, D_{so}^2/4\, L_{axial}} \tag{39}$$

According to Fig. 4, the proposed PMSG (current load 200 A/cm) is near the minimum outer diameter point, however this point is not coincident with the maximum power density point (Fig. 5). It should be noted that, as stated in Table II, the axial length of the generator is proportional to the gap diameter, instead of the outer diameter, so minimizing the outer volume (or maximizing power density) is not the same as minimizing the outer diameter. In any case, both points are close to each other.

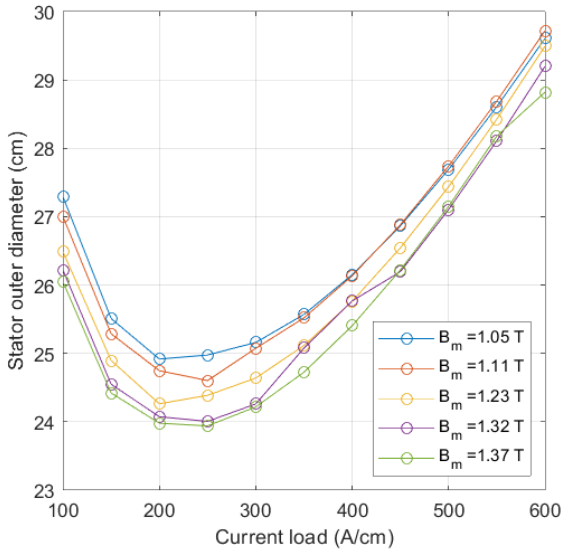

Fig. 4. Parametric study on the stator outer diameter

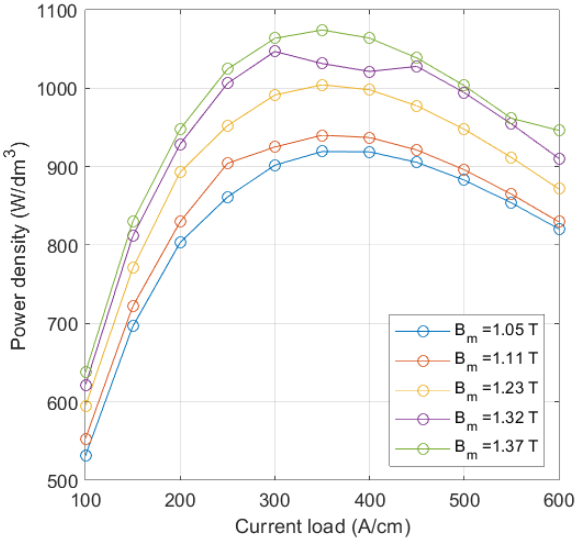

Fig. 5. Parametric study on the power density

4. Finite Element Model

The PMSG has been simulated with the finite element method using FluxMotor from Altair. Table VI shows a comparison of some of the calculated values, and it is shown that the FEM results are in accordance with the analytical calculations. The no-load air gap flux density is shown in Fig. 6, it is close to a rectangular waveform under PMs. The main source of divergence between analytical and FEM results are the iron losses, as the analytical formulae are only a rude approximation and the flux density distribution is nor uniform (Fig. 7). Furthermore, the stator and rotor yokes are not saturated, nor the stator teeth, as the flux density is lower than the limit value. The working point at the rated speed is defined as shown in Fig. 8, being J the rated current and ψ is the control angle. The rated current is 18 A, according to (7) and the control angle has been set as 50°.

Table VI. - Comparison between the analytical and FEM results

SIMULATION	SYMBOL	ANALYTICAL VALUE	FEM VALUE
Design	S_s (mm^2)	120.28	120.36
	k_{fill} (%)	40	40.92
	R (ohm)	0.689	0.685
Open circuit	E_{01} (V)	300.22	283.61
	$\hat{B}_g$ (T)	0.8658	0.8429
	$\hat{B}_{g1}$ (T)	1.0648	1.037
	$\hat{\psi}_{01}$ (T)	1.352	1.394
Working point	P_{Cu} (W)	673	668
	P_{Fe} (W/kg)	1.31	1.43
	P_{Fe} (W)	84.89	64.34
	η (%)	92.42	92.14

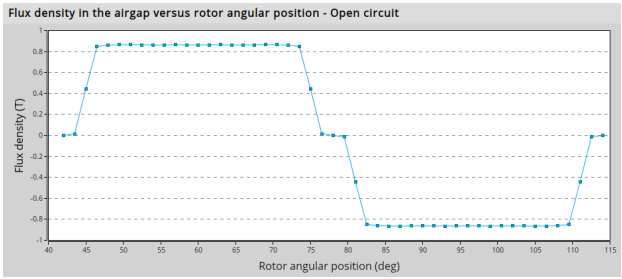

Fig. 6. No-load air gap flux density versus rotor angular position

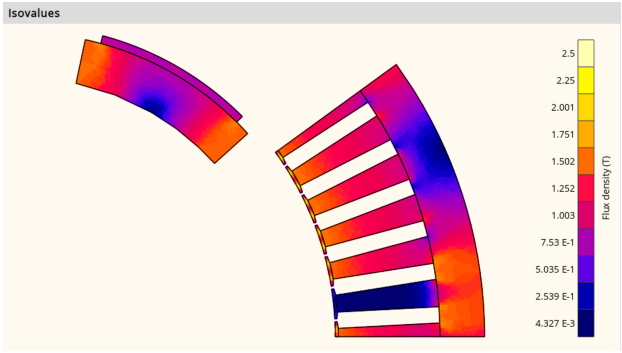

Fig. 7. Flux density map

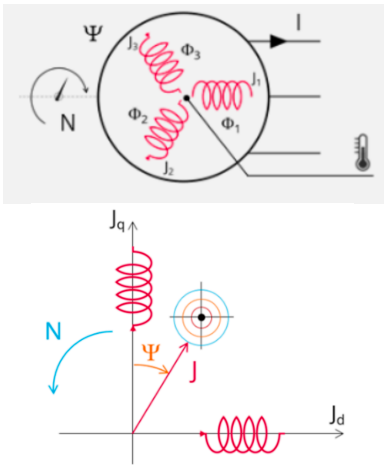

Fig. 8. Working point scheme of the generator, as shown in FluxMotor

5. Conclusion

This paper focuses on permanent magnet synchronous generators for small-scale wind power applications. A design methodology based on sizing equations is presented, and then the analytical model is validated using the finite element method.

The diameter-cubed sizing equation considers the effects of the magnetic field waveforms through the permanent magnets or winding factor. The effects of the stator slots are also included by use of the Carter factor.

The analytical and finite element models show good agreement, both with no load and under load. The generator is unsaturated and the iron losses are only a small fraction of the losses, so the non uniform distribution of the magnetic flux density can be neglected for the efficiency calculation.

Acknowledgement

This publication is part of the project TED2021-129801B-I00 funded by MCIN/AEI/10.13039/501100011033 and by European Union Next Generation EU/PRTR.

This work has also been supported in part by the Spanish Ministry of Universities under Grant FPU20/03436.

References

[1] K. Calautit, A. Aquino, J. K. Calautit, P. Nejat, F. Jomehzadeh, and B. R. Hughes, “A Review of Numerical Modelling of Multi-Scale Wind Turbines and Their Environment,” *Comput. 2018, Vol. 6, Page 24*, vol. 6, no. 1, p. 24, Mar. 2018.

[2] C. Wang and R. G. Prinn, “Potential climatic impacts and reliability of very large-scale wind farms,” *Atmos. Chem. Phys.*, vol. 10, no. 4, pp. 2053–2061, 2010.

[3] B. H. Fiedler and M. S. Bukovsky, “The effect of a giant wind farm on precipitation in a regional climate model,” *Environ. Res. Lett.*, vol. 6, no. 4, p. 045101, Oct. 2011.

[4] A. Tummala, R. K. Velamati, D. K. Sinha, V. Indraja, and V. H. Krishna, “A review on small scale wind turbines,” *Renew. Sustain. Energy Rev.*, vol. 56, pp. 1351–1371, Apr. 2016.

[5] N. Goudarzi and W. D. Zhu, “A review on the development of wind turbine generators across the world,” *Int. J. Dyn. Control*, vol. 1, no. 2, pp. 192–202, Jun. 2013.

[6] T. Gönen, *Electrical Machines with MATLAB*, 2nd ed. Boca Raton: CRC Press, 2012.

[7] Y. Du and A. K. S. Bhat, “Power converter schemes for small scale wind energy conversion systems - Review, a systematic classification based on isolation transformer and generator side rectifier,” *Proc. - 2016 2nd Int. Conf. Comput. Intell. Commun. Technol. CICT 2016*, pp. 338–344, Aug. 2016.

[8] K. Wirtayasa, P. Irasari, M. Kasim, P. Widiyanto, and M. Hikmawan, “Design of an axial-flux permanent-magnet generator(AFPMG) 1 kW, 220 volt, 300 rpm, 1 phase for pico hydro power plants,” *Proceeding - ICSEEA 2017 Int. Conf. Sustain. Energy Eng. Appl. "Continuous Improv. Sustain. Energy Eco-Mobility"*, vol. 2018-January, pp. 172–179, Jul. 2017.

[9] K. Wirtayasa, P. Irasari, P. Widiyanto, and M. F. Hikmawan, "Design of three-phase axial flux permanent magnet generator double-side internal rotor for high-speed application," *Proc. - 6th Int. Conf. Sustain. Energy Eng. Appl. ICSEEA 2018*, pp. 174–179, Jan. 2019.

[10] K. Latoufis, K. Troullaki, T. Pazios, and N. Hatziargyriou, "Design of axial flux permanent magnet generators using various magnetic materials in locally manufactured small wind turbines," *Proc. - 2016 22nd Int. Conf. Electr. Mach. ICEM 2016*, pp. 1545–1551, Nov. 2016.

[11] K. Latoufis, T. Pazios, K. Chira, N. Korres, and N. Hatziargyriou, "Open Design and Local Manufacturing of Small Wind Turbines: Case Studies in Ethiopia and Nepal," *2018 IEEE PES/IAS PowerAfrica, PowerAfrica 2018*, pp. 148–153, Nov. 2018.

[12] M. Bonnet, Y. Lefevre, J. F. Llibre, D. Harribey, and F. Defay, "Model of an Ironless Axial Flux Permanent Magnet Motor Based on the Field Produced by a Single Magnet," *IEEE Trans. Magn.*, vol. 57, no. 7, Jul. 2021.

[13] M. Bonnet, J. F. Llibre, D. Harribey, and Y. Lefèvre, "Ironless Axial Flux Wind Turbine Motor with Two Cylindrical Magnet Rings," *2022 Int. Conf. Electr. Mach. ICEM 2022*, pp. 1941–1947, 2022.

[14] A. A. Pop, F. Jurca, C. Oprea, M. Chirca, S. Breban, and M. M. Radulescu, "Axial-flux vs. radial-flux permanent-magnet synchronous generators for micro-wind turbine application," *2013 15th Eur. Conf. Power Electron. Appl. EPE 2013*, 2013.

[15] R. Kumar *et al.*, "A Review on Transverse Flux Permanent Magnet Machines for Wind Power Applications," *IEEE Access*, vol. 8, pp. 216543–216565, 2020.

[16] S. O. Ani, H. Polinder, and J. A. Ferreira, "Small wind power generation using automotive alternator," *Renew. Energy*, vol. 66, pp. 185–195, Jun. 2014.

[17] J. S. Artal-Sevil, R. Dufo, J. A. Dominguez, and J. L. Bernal-Agustin, "Small wind turbines in smart grids. Transformation of electrical machines in permanent magnet synchronous generators," *2018 13th Int. Conf. Ecol. Veh. Renew. Energies, EVER 2018*, pp. 1–8, May 2018.

[18] V. Ballestín-Bernad, J. S. Artal-Sevil, J. A. Domínguez-Navarro, and J. L. Bernal-Agustín, "Low-cost variable-speed wind turbines design by recycling small electrical machines. Arrangement of permanent magnets in the rotor.," *Renew. Energy Power Qual. J.*, vol. 20, pp. 833–838, Sep. 2022.